A&A 588, A35 (2016)
DOI: 10.1051/0004-6361/201528059

Astronomy & Astrophysics

The white dwarf population within 40 pc of the Sun

Santiago Torres[1,2] and Enrique García-Berro[1,2]

[1] Departament de Física, Universitat Politècnica de Catalunya, c/Esteve Terrades 5, 08860 Castelldefels, Spain
e-mail: enrique.garcia-berro@upc.edu
[2] Institute for Space Studies of Catalonia, c/Gran Capita 2–4, Edif. Nexus 201, 08034 Barcelona, Spain

Received 29 December 2015 / Accepted 7 February 2016

ABSTRACT

Context. The white dwarf luminosity function is an important tool to understand the properties of the solar neighborhood, like its star formation history, and its age.
Aims. Here we present a population synthesis study of the white dwarf population within 40 pc from the Sun, and compare the results of this study with the properties of the observed sample.
Methods. We use a state-of-the-art population synthesis code based on Monte Carlo techniques, which incorporates the most recent and reliable white dwarf cooling sequences, an accurate description of the Galactic neighborhood, and a realistic treatment of all the known observational biases and selection procedures.
Results. We find a good agreement between our theoretical models and the observed data. In particular, our simulations reproduce a previously unexplained feature of the bright branch of the white dwarf luminosity function, which we argue is due to a recent episode of star formation. We also derive the age of the solar neighborhood employing the position of the observed cut-off of the white dwarf luminosity function, to obtain $\sim 8.9 \pm 0.2$ Gyr.
Conclusions. We conclude that a detailed description of the ensemble properties of the population of white dwarfs within 40 pc of the Sun allows us to obtain interesting constraints on the history of the Solar neighborhood.

Key words. white dwarfs – stars: luminosity function, mass function – Galaxy: evolution

1. Introduction

White dwarfs are the most common stellar evolutionary endpoint (Althaus et al. 2010). Actually, all stars with masses smaller than $\sim 10\,M_{\odot}$ will end their lives as white dwarfs (García-Berro et al. 1997; Poelarends et al. 2008). Hence, given the shape of the initial mass function, the local population of white dwarfs carries crucial information about the physical processes that govern the evolution of the vast majority of stars and, in particular, of the total amount of mass lost by low- and intermediate-mass stars during the red giant and asymptotic giant branch evolutionary phases. Also, the population of white dwarfs carries fundamental information about the history, structure, and properties of the solar neighborhood, and specifically about its star formation history and age. Clearly, obtaining all this information from the observed ensemble properties of the white dwarf population is an important endeavour.

However, to obtain useful information from the ensemble characteristics of the white dwarf population three conditions must be met. Firstly, extensive and accurate observational data sets are needed. In particular, individual spectra of a sufficiently large number of white dwarfs are needed. This has been possible recently, with the advent of large-scale automated surveys, which routinely obtain reliable spectra for sizable samples of white dwarfs. Examples of these surveys, although not the only ones, are the Sloan Digital Sky Survey (York et al. 2000), and the SuperCOSMOS Sky Survey (Rowell & Hambly 2011), which have allowed us to obtain extensive observational data for a very large number of white dwarfs. Secondly, improved models of the atmospheres of white dwarfs that allow us to model their spectra – thus granting us unambiguous determinations of their atmospheric composition, and accurate measurements of their surface gravities and effective temperatures – are also needed. Over recent years, several model atmosphere grids with increasing levels of detail and sophistication have been released (Bergeron et al. 1992; Koester et al. 2001; Kowalski & Saumon 2006; Tremblay et al. 2011, 2013), thus providing us with a consistent framework with which to analyze the observational results. Finally, it is also essential to have state-of-the-art white dwarf evolutionary sequences to determine their individual ages. With this in mind, it is worth mentioning that we now understand relatively well the physics controlling the evolution of white dwarfs. In particular, it has been known for several decades now that the evolution of white dwarfs is determined by a simple gravothermal process. However, although the basic picture of white dwarf evolution has remained unchanged for some time, we now have very reliable and accurate evolutionary tracks, which take into account all the relevant physical processes involved in their cooling, and which allow us to determine the precise ages of individual white dwarfs (Salaris et al. 2010; Renedo et al. 2010). Furthermore, it is worth emphasizing that the individual ages derived in this way are nowadays as accurate as main-sequence ages (Salaris et al. 2013). When all these conditions are met, useful information can be obtained from the observed data. Accordingly, significant efforts have recently been invested in successfully modeling the observed properties of several white dwarf populations with a high degree of realism. These include the Galactic disk and halo – see the very recent works of Cojocaru et al. (2014, 2015) and references therein – and the system of Galactic open

(García-Berro et al. 2010; Bellini et al. 2010; Bedin et al. 2010) and globular clusters (Hansen et al. 2002; García-Berro et al. 2014; Torres et al. 2015).

In this paper we analyze the properties of the sample of local disk white dwarfs, namely the sample of stars with distances smaller than 40 pc (Limoges et al. 2013, 2015). The most salient features of this sample of white dwarfs are discussed in Sect. 2. We then employ a Monte Carlo technique to model the observed properties of the local sample of white dwarfs. Our Monte Carlo simulator is described in some detail in Sect. 3. The results of our population synthesis studies are then described in Sect. 4. In this section we discuss the effects of the selection criteria (Sect. 4.1), we calculate the age of the Galactic disk (Sect. 4.2), we derive the star formation history of the solar neighborhood (Sect. 4.3), and we determine the sensitivity of this age determination to the slope of the initial mass function and to the adopted initial-to-final mass relationship (Sect. 4.4). Finally, in Sect. 5, we summarize our main results and we draw our conclusions.

2. The observational sample

Over the last decades several surveys have provided us with different samples of disk white dwarfs. Hot white dwarfs are preferentially detected using ultraviolet color excesses. The Palomar Green Survey (Green et al. 1986) and the Kiso Schmidt Survey (Kondo et al. 1984) used this technique to study the population of hot disk white dwarfs. However, these surveys failed to probe the characteristics of the population of faint, hence cool and redder, white dwarfs. Cool disk white dwarfs are also normally detected in proper motion surveys (Liebert et al. 1988), thus allowing us to probe the faint end of the luminosity function, and to determine the position of its cut-off. Unfortunately, the number of white dwarfs in the faintest luminosity bins represents a serious problem. Other recent magnitude-limited surveys, like the Sloan Digital Sky Survey (SDSS), were able to detect many faint white dwarfs, thus enabling us to determine a white dwarf luminosity function that covers the entire range of interest of magnitudes, namely $7 \lesssim M_{\rm bol} \lesssim 16$ (Harris et al. 2006). However, the sample of Harris et al. (2006) is severely affected by observational biases, completeness corrections and selection procedures. Holberg et al. (2008) showed that the best way to overcome these observational drawbacks is to rely on volume-limited samples. Accordingly, Holberg et al. (2008) and Giammichele et al. (2012) studied the white dwarf population within 20 pc of the Sun, and measured the properties of an unbiased sample of ∼130 white dwarfs. The completeness of their samples is ∼90%. More recently, Limoges et al. (2013) and Limoges et al. (2015) have derived the ensemble properties of a sample of ∼500 white dwarfs within 40 pc of the Sun, using the results of the SUPERBLINK survey, which is a survey of stars with proper motions larger than 40 mas yr^{-1} (Lépine & Shara 2005). The estimated completeness of the white dwarf sample derived from this survey is ∼70%, thus allowing for a meaningful statistical analysis. We compare the results of our theoretical simulations with the white dwarf luminosity function derived from this sample. However, a few cautionary remarks are necessary. First, this luminosity function has been obtained from a spectroscopic survey that has not yet been completed. Second, the photometry is not yet optimal. Finally, and most importantly, trigonometric parallaxes are not available for most cool white dwarfs in the sample, preventing accurate determinations of atmospheric parameters and radii (hence, masses) of each individual white dwarf. For these stars Limoges et al. (2015) were forced to assume a mass of $0.6\,M_{\odot}$. All in all, the luminosity function of Limoges et al. (2015) is still somewhat preliminary, but nevertheless is the only one based on a volume-limited sample that extends out to 40 pc. Nevertheless, we explore the effects of these issues below in Sects. 4.1 and 4.2.

3. The population synthesis code

A detailed description of the main ingredients employed in our Monte Carlo population synthesis code can be found in our previous works (García-Berro et al. 1999, 2004; Torres et al. 2001, 2002). Not withstanding, in the interest of completeness, we summarize its main important features.

The simulations described below were performed using the generator of random numbers of James (1990). This algorithm provides a uniform probability density within the interval $(0, 1)$, ensuring a repetition period of $\gtrsim 10^{18}$, which for practical applications is virtually infinite. When Gaussian probability distributions were needed we employed the Box-Muller algorithm (Press et al. 1986). For each of the synthetic white dwarf populations described below, we generated 50 independent Monte Carlo simulations which employ different initial seeds. Furthermore, for each of these Monte Carlo realizations, we increased the number of simulated Monte Carlo realizations to 10^4 using bootstrap techniques – see Camacho et al. (2014) for details. In this way convergence in all the final values of the relevant quantities, can be ensured. In the next sections we present the ensemble average of the different Monte Carlo realizations for each quantity of interest, as well as the corresponding standard deviation. Finally, we mention that the total number of synthetic stars of the restricted samples described below and the observed sample are always similar. In this way we guarantee that the comparison of both sets of data are statistically sound.

To produce a consistent white dwarf population, we first generated a set of random positions of synthetic white dwarfs in a spherical region centered on the Sun, adopting a radius of 50 pc. We used a double exponential distribution for the local density of stars. For this density distribution we adopted a constant Galactic scale height of 250 pc and a constant scale length of 3.5 kpc. The time at which each synthetic star was born for our initial model was generated according to a constant star formation rate, and adopting an age of the Galactic disk age, $t_{\rm disk}$. The mass of each star was drawn according to a Salpeter mass function (Salpeter 1955) with exponent $\alpha = 2.35$, unless otherwise stated, which, for the relevant range of masses, is totally equivalent to the standard initial mass function of Kroupa (2001). Velocities were chosen randomly, taking into account the differential rotation of the Galaxy, the peculiar velocity of the Sun, and a dispersion law that depends on the scale height (García-Berro et al. 1999). The evolutionary ages of the progenitors were those of Renedo et al. (2010). Given the age of the Galaxy and the age, metallicity, and mass of the progenitor star, we know which synthetic stars have had time to become white dwarfs, and for these, we derive their mass using the initial-final mass relationship of Catalán et al. (2008a), except otherwise stated. We also assign a spectral type to each of the artificial stars. In particular, we adopt a fraction of 20% of white dwarfs with hydrogen-deficient atmospheres, while the rest of the stars are assumed to be of DA spectral type.

The set of adopted cooling sequences employed here encompasses the most recent evolutionary calculations for different white dwarf masses. For white dwarf masses smaller than $1.1\,M_{\odot}$ we adopted the cooling tracks of white dwarfs with carbon-oxygen cores of Renedo et al. (2010) for stars

with hydrogen-dominated atmospheres and those of Benvenuto & Althaus (1997) for hydrogen-deficient envelopes. For white dwarf masses larger than this value we used the evolutionary results for oxygen-neon white dwarfs of Althaus et al. (2007) and Althaus et al. (2005). Finally, we interpolated the luminosity, effective temperature, and the value of $\log g$ of each synthetic star using the corresponding white dwarf evolutionary tracks . Additionally, we also interpolated their *UBVRI* colors, which we then converted to the ugriz color system.

4. Results

4.1. The effects of the selection criteria

A key point in the comparison of a synthetic population of white dwarfs with the observed data is the implementation of the observational selection criteria in the theoretical samples. To account for the observational biases with a high degree of fidelity, we implemented the selection criteria employed by Limoges et al. (2013, 2015) in their analysis of the SUPERBLINK database in a strict way. Specifically, we only considered objects in the northern hemisphere ($\delta > 0°$) up to a distance of 40 pc, and with proper motions larger than $\mu > 40\,\mathrm{mas\,yr^{-1}}$. Then, we introduced a cut in the reduced proper motion diagram ($H_g, g-z$) as Limoges et al. (2013) did – see their Fig. 1 – eliminating from the synthetic sample of white dwarfs those objects with $H_g > 3.56(g-z) + 15.2$, which are outside of the location where, presumably, white dwarfs should be found. Finally, we only took those stars with magnitudes brighter than $V = 19$ into consideration.

In Fig. 1, we show the effects of these last two cuts on the entire population of white dwarfs for our fiducial model. In particular, in the top panel of this figure, the reduced proper motion diagram ($H_g, g-z$) of the theoretical white dwarf population (black dots) and the corresponding selection criteria (red dashed lines) are displayed. As can be seen, the overall effect of this selection criterion is that the selected sample is, on average, redder than the population from which it is drawn, independent of the adopted age of the disk. Additionally, in the bottom panel of Fig. 1, we plot the bolometric magnitudes of the individual white dwarfs as a function of their distance for the synthetic white dwarf population. The red dashed line represents the selection cut in magnitude, $V = 19$. It is clear that this cut eliminates faint and distant objects. Also, it is evident that the number of synthetic white dwarfs increases smoothly for increasing magnitudes up to $M_{\rm bol} \approx 15.0$, and that for magnitudes larger than this value there is a dramatic drop in the white dwarf number counts. Furthermore, for distances of ∼40 pc the observational magnitude cut will eliminate all white dwarfs with bolometric magnitudes larger than $M_{\rm bol} \approx 16.0$. However, this magnitude cut still enables us to resolve the sharp drop-off in the number counts of white dwarfs at magnitude $M_{\rm bol} \approx 15.0$. This, in turn, is important since, as shown below, it will enable us to unambigously determine the age of the Galactic disk.

We now study if our modeling of the selection criteria is robust enough. This is an important issue because reliable ugriz photometry was only available for a subset of the SUPERBLINK catalog. Consequently, Limoges et al. (2015) use photometric data from other sources like 2MASS, Galex, and USNO-B1.0 – see Limoges et al. (2013) for details. It is unclear how this procedure may affect the observed sample. Obviously, simulating all the specific observational procedures is too complicated for the purpose of the present analysis, but we did conduct two supplementary sets of simulations to assess the reliability of our

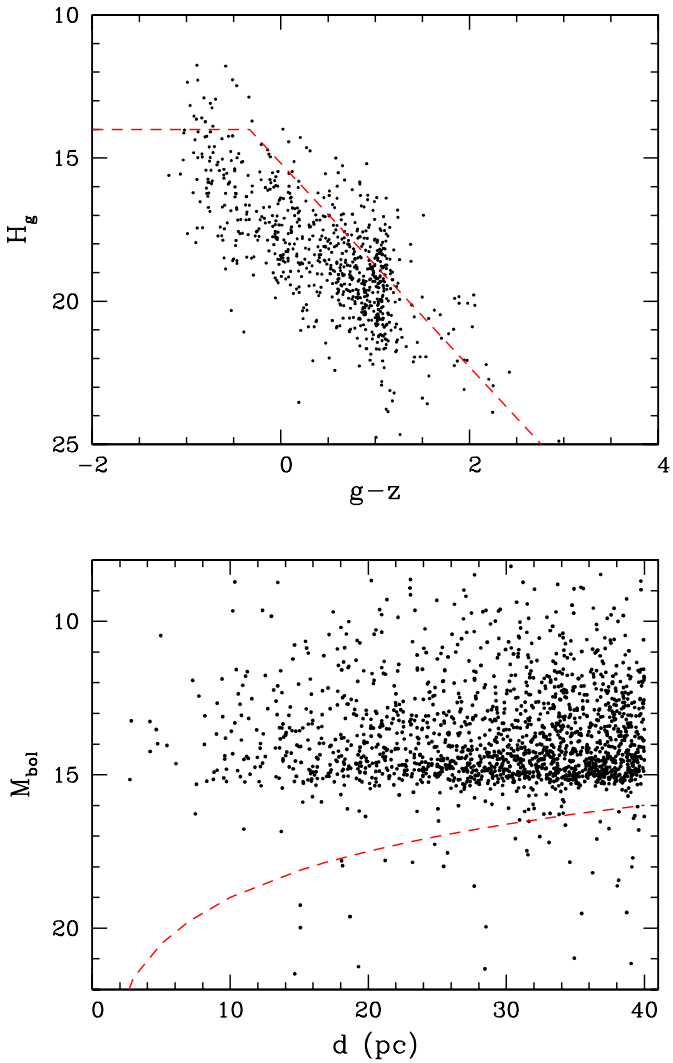

Fig. 1. *Top panel*: effects of the reduced proper motion diagram cut on the synthetic population of white dwarfs. *Bottom panel*: effects of the cut in V magnitude on the simulated white dwarf population. In both panels the synthetic white dwarfs are shown as solid dots, whereas the red dashed lines represent the selection cut.

results. In the first of these sets we discarded an additional fraction of white dwarfs in the theoretical samples that were obtained after applying all the selection criteria previously described. We found that if the percentage of discarded synthetic stars is $\lesssim$15%, the results described below remain unaffected. Additionally, in a second set of simulations, we explored the possibility that the sample of Limoges et al. (2015) is indeed larger than that used to compute the theoretical luminosity function. Accordingly, we artificially increased the number of synthetic white dwarfs which pass the successive selection criteria in the reduced proper motion diagram. In particular, we increased by 15% the number of artificial white dwarfs populating the lowest luminosity bins of the luminosity function (those with $M_{\rm bol} > 12$). Again, we found that the differences between both sets of simulations – our reference simulation and this one – were minor.

Once the effects of the observational biases and selection criteria have been analyzed, a theoretical white dwarf luminosity function can be built and compared to the observed one. To allow for a meaningful comparison between the theoretical and the observational results, we grouped the synthetic white dwarfs using the same magnitude bins employed by Limoges et al. (2015). We

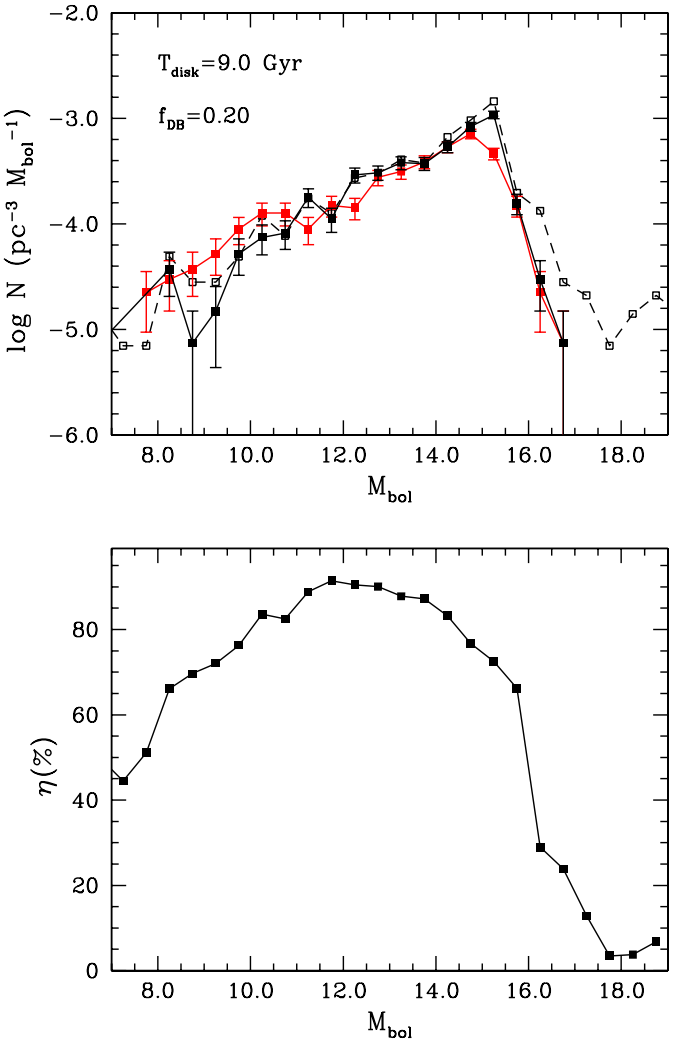

Fig. 2. *Top panel*: synthetic white dwarf luminosity functions (black lines) compared to the observed luminosity function (red line). The solid line shows the luminosity function of the simulated white dwarf population when all the selection criteria have been considered, while the dashed line displays the luminosity function of the entire sample. *Bottom panel*: completeness of white dwarf population for our reference model.

emphasize that the procedure employed by Limoges et al. (2015) to derive the white dwarf luminosity function simply consists in counting the number of stars in each magnitude bin, given that their sample is volume-limited. That is, in principle, their number counts should correspond with the true number density of objects per bolometric magnitude and unit volume – provided that their sample is complete, without the need for correcting the number counts using the $1/V_{\rm max}$ method – or an equivalent method – as occurs for magnitude and proper motion limited samples.

In the top panel of Fig. 2 the theoretical results are shown using black lines, while the observed luminosity function is displayed using a red line. Specifically, for our reference model we show the number of white dwarfs per unit bolometric magnitude and volume for the entire theoretical white dwarf population when no selection criteria are employed – dashed line and open squares – and the luminosity function obtained when the selection criteria previously described are used – solid line and filled squares. It is worthwhile mentioning here that the theoretical luminosity functions have been normalized to the bin of bolometric magnitude $M_{\rm bol} = 14.75$, which corresponds to the magnitude bin for which the observed white dwarf luminosity function has the smallest error bars. Thus, since this luminosity bin is very close to the maximum of the luminosity function, the normalization criterion is practically equivalent to a number density normalization. As clearly seen in this figure, the theoretical results match very well the observed data, except for a quite apparent excess of hot white dwarfs, which is discussed in detail below. We note as well that the selection criteria employed by Limoges et al. (2015) basically affect the low luminosity tail of the white dwarf luminosity function, but not the location of the observed drop-off in the white dwarf number counts, nor that of the maximum of the luminosity function. This can be more easily seen by looking at the bottom panel of Fig. 2, where the completeness of the simulated restricted sample is shown. We found that the completeness of the entire sample is 78%. However, the restricted sample is nearly complete at intermediate bolometric magnitudes – between $M_{\rm bol} \simeq 10$ and 15 – but decreases very rapidly for magnitudes larger than $M_{\rm bol} = 15$, a clear effect of the selection procedure employed by Limoges et al. (2015). Nevertheless, this low-luminosity tail is populated preferentially by helium-atmosphere stars and by very massive oxygen-neon white dwarfs. The prevalence of helium-atmosphere white dwarfs at low luminosities is due to the fact that stars with hydrogen-deficient atmospheres have lower luminosities than their hydrogen-rich counterparts of the same mass and age, because in their atmospheres collision-induced absorption does not play a significant role and cool to a very good approximation as black bodies. Also, the presence of massive oxygen-neon white dwarfs is a consequence of their enhanced cooling rate, owing to their smaller heat capacity.

4.2. Fitting the age

Now we estimate the age of the disk using the standard method of fitting the position of the cut-off of the white dwarf luminosity function. We did this by comparing the faint end of the observed white dwarf luminosity function with our synthetic luminosity functions. Despite the fact that the completeness of the faintest bins of the luminosity function is substantially smaller (below ~60%), we demonstrated in the previous section that the position of the cut-off remains almost completely unaffected by the selection procedures. Accordingly, we ran a set of Monte Carlo simulations for a wide range of disk ages. We then employed a χ^2 test in which we compared the theoretical and observed number counts of the bins that define the cut-off, namely the three last bins (those with $M_{\rm bol} > 15.5$) of the luminosity function. In the top panel of Fig. 3 we plot this probability as a function of the disk age. The best fit is obtained for an age of 8.9 Gyr, and the width of the distribution at half-maximum is 0.4 Gyr. The bottom panel of this figure shows the white dwarf luminosity function for the best-fit age.

One possible concern could be that the age derived in this way could be affected by the assumption that the mass of cool white dwarfs for which no trigonometric parallax could be measured was arbitrarily assumed to be $0.6\,M_{\odot}$. This may have an impact on the age determination using the cut-off of the white dwarf luminosity function. To assess this issue, we conducted an additional simulation in which all synthetic white dwarfs with cooling times longer than 1 Gyr have this mass. We then computed the new luminosity function and derived the corresponding age estimate. We found that the difference in ages between both calculations is smaller than 0.1 Gyr.

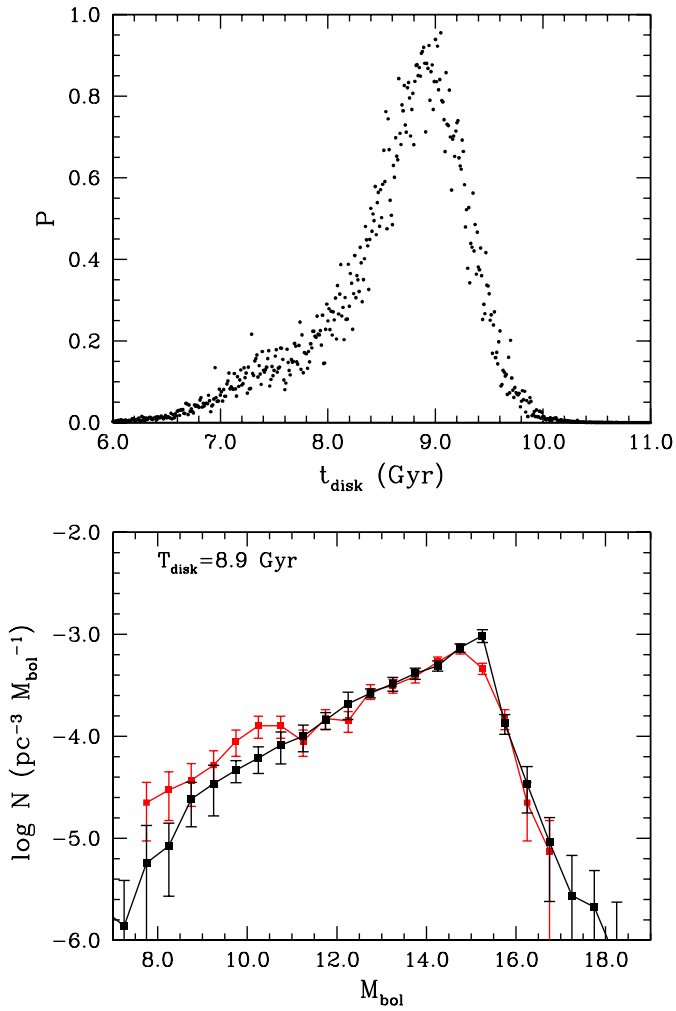

Fig. 3. *Top panel*: χ^2 probability test as a function of the age obtained by fitting the three faintest bins defining the cut-off of the white dwarf luminosity function. *Bottom panel*: white dwarf luminosity function for the best-fit age.

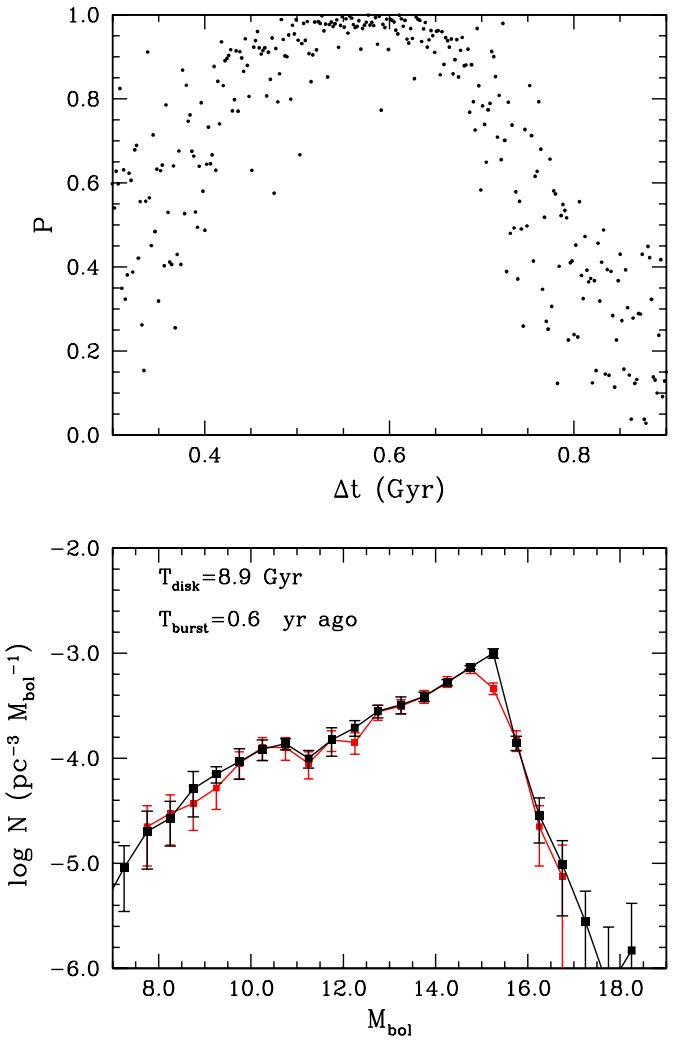

Fig. 4. *Top panel*: χ^2 probability test as a function of the age of the burst of star formation obtained by fitting the nine brightest bins of the white dwarf luminosity function. *Bottom panel*: synthetic white dwarf luminosity function for a disk age of 8.9 Gyr and a recent burst of star formation (black line), compared with the observed white dwarf luminosity function of (red lines).

4.3. A recent burst of star formation

As clearly shown in the bottom panel of Fig. 3 the agreement between the theoretical simulations and the observed results is very good except for the brightest bins of the white dwarf luminosity, namely those with $M_{\rm bol} \lesssim 11$. Also, our simulations fail to reproduce the shape of the peak of the luminosity function, an aspect which we investigate in more detail in Sect. 4.4. The excess of white dwarfs for the brightest luminosity bins is statistically significant, as already noted by Limoges et al. (2015). Limoges et al. (2015) have already discussed various possibilities and pointed out that the most likely one is that this feature of the white dwarf luminosity function might be due to a recent burst of star formation. Noh & Scalo (1990) demonstrated some time ago that a burst of star formation generally produces a bump in the luminosity function, and that the position of the bump on the hot branch of the luminosity function is ultimately dictated by the age of the burst of star formation – see also Rowell (2013).

Based on these considerations, we explored the possibility of a recent burst of star formation by adopting a burst that occurred some time ago but which is still active today. The strength of this episode of star formation is another parameter that can be varied. We thus ran our Monte Carlo simulator using a fixed age of the disk of 8.9 Gyr and considered the time elapsed since the beginning of the burst, Δt, and its strength as adjustable parameters. The top panel of Fig. 4 shows the probability distribution for Δt, computed using the same procedure that was employed to derive the age of the solar neighborhood, but adopting the nine brightest bins of the white dwarf luminosity function, which correspond to the location of the bump of the white dwarf luminosity function. The best fit is obtained for a burst that happened $\sim 0.6 \pm 0.2$ Gyr ago and is ~ 5 times stronger than the constant star formation rate that was adopted in the previous section. As can be seen in this figure the probability distribution function does not have a clear Gaussian shape. Moreover, the maximum of the probability distribution is flat, and the dispersion is quite high, meaning that the current observational data set prevents us from constraining the properties of this episode of star formation in an effective way. However, when this episode of star formation is included in the calculations the agreement between the theoretical calculations and the observational results is excellent. This is clearly shown in the bottom panel of Fig. 4, where we show our best-fit model, and compare it with the observed white dwarf luminosity function of Limoges et al. (2015). As can be

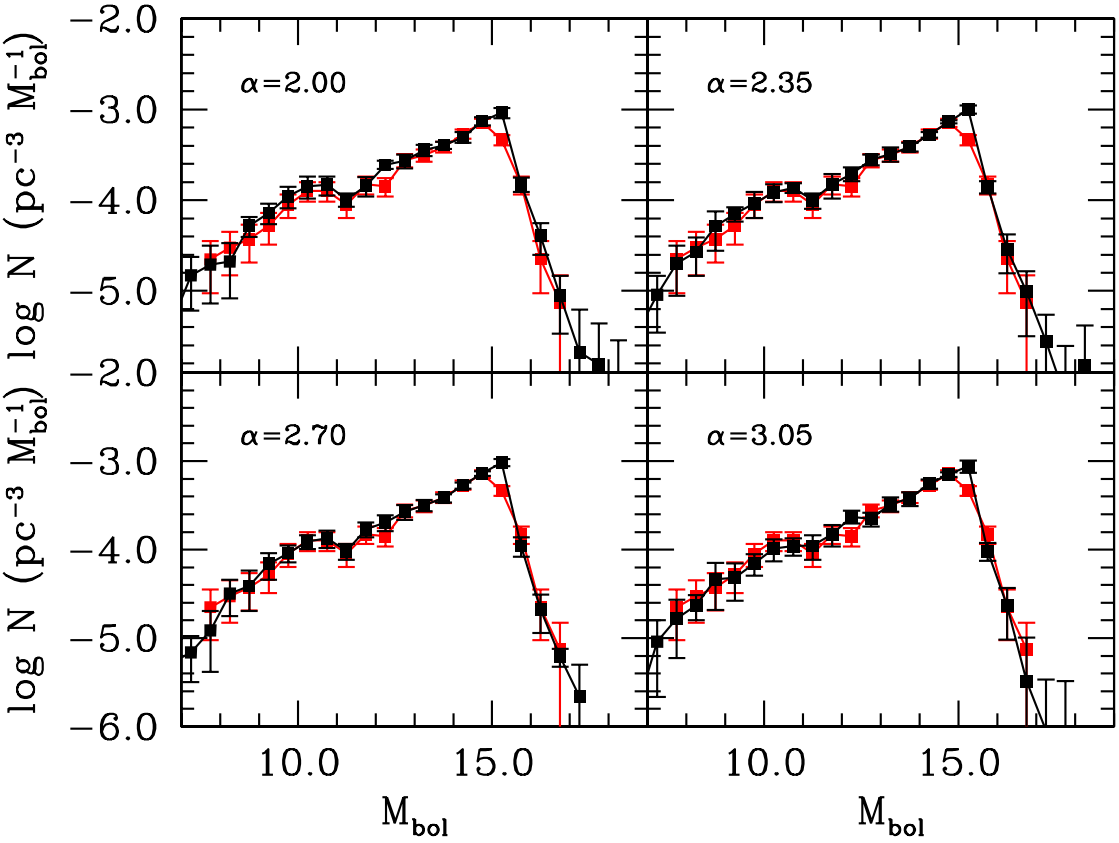

Fig. 5. Synthetic white dwarf luminosity function for a disk age of 8.9 Gyr and a recent burst of star formation for different values of the slope of the Salpeter IMF (black lines), compared with the observed white dwarf luminosity function of Limoges et al. (2015) – red line.

seen, the observed excess of hot white dwarfs is now perfectly reproduced by the theoretical calculations.

4.4. Sensitivity of the age to the inputs

In this section we compare the sensitivity of the age determination that was obtained in Sect. 4.2 to the most important inputs adopted in our simulations. We start discussing the sensitivity of the age to the slope of initial mass function. This is done with the help of Fig. 5, where we compare the theoretical white dwarf luminosity functions that were obtained with different values of the exponent α for a Salpeter-like initial mass function with the observed luminosity function. As can be seen, the differences between the different luminosity functions are minimal. Moreover, the value of α has no influence on the precise location of the cut-off of the luminosity function, hence we conclude that the age determination is insensitive to the adopted initial mass function.

In a second step we studied the sensitivity of the age determination to the initial-to-final mass relationship. As mentioned before, we used the results of Catalán et al. (2008a,b) for our reference calculation. To model different slopes of the initial-to-final mass relationships we multiplied the resulting final mass that was obtained with the relationship of Catalán et al. (2008a) by a constant factor, β – see Fig. 6. This choice is motivated by the fact that most semi-empirical and theoretical initial-to-final mass relationships have similar shapes – see, for instance, Fig. 2 of Renedo et al. (2010) and Fig. 23 of Andrews et al. (2015). Figure 7 displays several theoretical luminosity functions that were obtained with different values of β. Clearly, the position of the cut-off of the white dwarf luminosity function remains

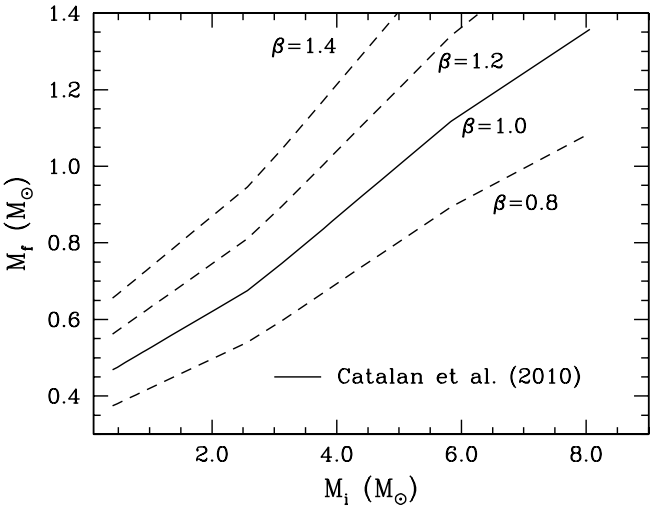

Fig. 6. Initial-final mass relationships adopted in this work. The solid line shows the semi-empirical initial-final mass relationship of Catalán et al. (2008b), while the dashed lines have been obtained by multiplying the final white dwarf mass by a constant factor β, as labeled.

almost unchanged, except for very extreme values of β. Thus, the age determination obtained previously is not severely affected by the choice of the initial-to-final mass function.

Nevertheless, Fig. 7 reveals one interesting point. As can be seen, large values of β result in better fits of the region near the maximum of the white dwarf luminosity function. This feature was already noted by Limoges et al. (2015) where they discussed several possibilities. In a first instance they discussed the

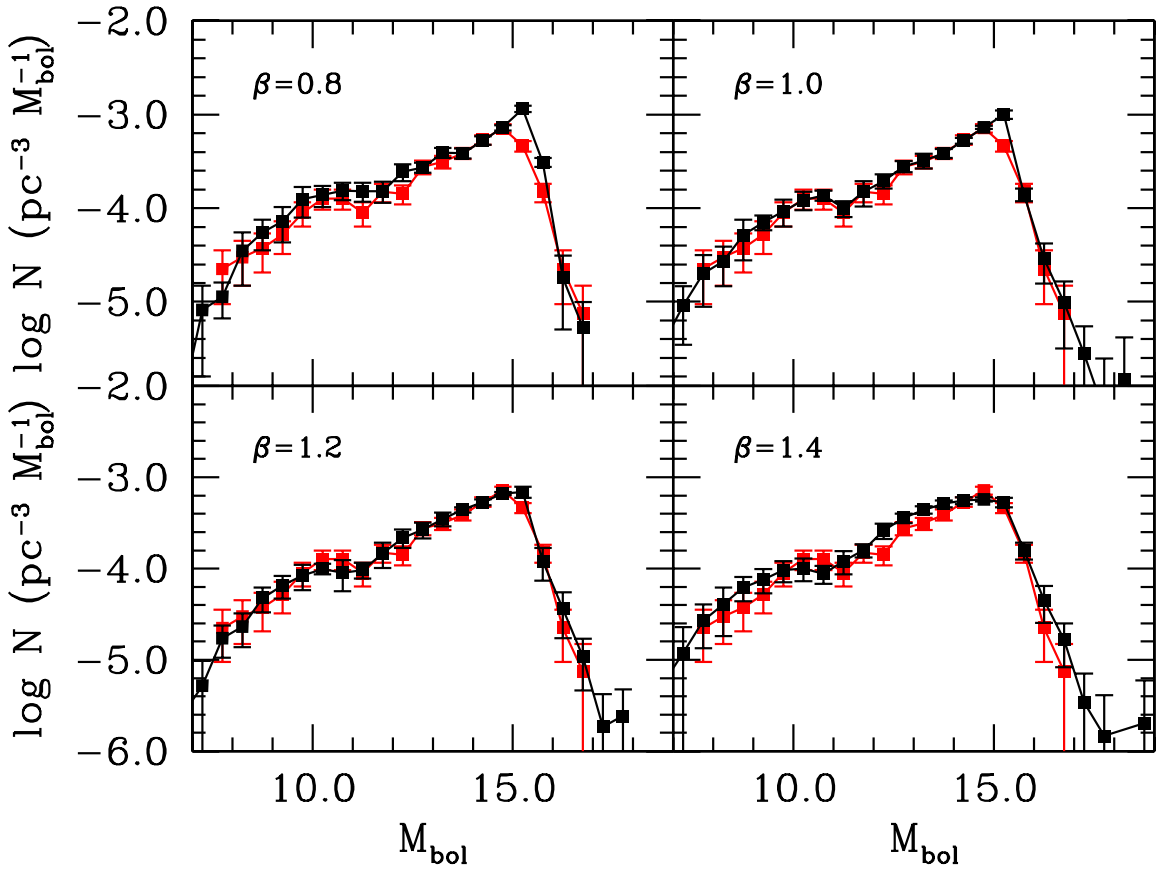

Fig. 7. Synthetic white dwarf luminosity function for a disk age of 8.9 Gyr and a recent burst of star formation for several choices of the initial-to-final mass relationship (black lines) compared with the observed white dwarf luminosity function of Limoges et al. (2015) – red lines. See text for details.

statistical relevance of this feature. They found that this discrepancy between the theoretical models and the observations could not be caused by the limitations of the observational sample, because the error bars in this magnitude region are small, and the completitude of the observed sample for these magnitudes is ∼80% (see Fig. 1). Thus, it seems quite unlikely that they lost so many white dwarfs in the survey. Another possibility could be that the cooling sequences for this range of magnitudes miss any important physical ingredient. However, at these luminosities cooling is dominated by convective coupling and crystallization (Fontaine et al. 2001). Since these processes are well understood and the cooling sequences in this magnitude range have been extensively tested in several circumstances with satisfactory results, it is also quite unlikely that this could be the reason for the discrepancy between theory and observations. Also, the initial mass function has virtually no effect on the shape of the maximum of the white dwarf luminosity function – see Fig. 5. Thus, the only possibility we are left with is the slope of the initial-to-final mass relationship. Figure 7 demonstrates that, to reproduce the shape of the maximum of the white dwarf luminosity function, $\beta = 1.2$ is needed. When such a extreme value of β is adopted we find that the synthetic restricted samples have clear excesses of massive white dwarfs. However, in general, massive white dwarfs have magnitudes beyond that of the maximum of the white dwarf luminosity function. Thus, a likely explanation of this lack of agreement between the theoretical models and the observations is that the initial-to-final mass relationship has a *steeper* slope for initial masses larger than $\sim 4\,M_{\odot}$. To check this possibility, we ran an additional simulation in which we adopted $\beta = 1.0$ for masses smaller than $4\,M_{\odot}$, and $\beta = 1.3$ otherwise. Adopting this procedure the excesses of massive white dwarfs disappear, while the fit to the white dwarf luminosity function is essentially the same as shown in the lower left panel of Fig. 7. Interestingly, the analysis of Dobbie et al. (2009) of massive white dwarfs in the open clusters NGC 3532 and NGC 2287 strongly suggests that, indeed, the slope of the initial-to-final-mass relationship for this mass range is steeper.

5. Summary, discussion, and conclusions

In this paper we studied the population of Galactic white dwarfs within 40 pc of the Sun, and we compared its characteristics with those of the observed sample of Limoges et al. (2015). We found that our simulations describe with good accuracy the properties of this sample of white dwarfs. Our results show that the completeness of the observed sample is typically ∼80%, although for bolometric magnitudes larger than ∼16 the completeness drops to much smaller values, of the order of 20% and even less, at lower luminosities. However, the cut-off of the observed luminosity function, which is located at $M_{\rm bol} \simeq 15$, is statistically significant. We then used the most reliable progenitor evolutionary times and cooling sequences to derive the age of the solar neighborhood, and found that it is $\simeq 8.9 \pm 0.2$ Gyr. This age estimate is robust, since it does not depend substantially on the most relevant inputs, like the slope of the initial mass function or the adopted initial-to-final mass relationship.

We also studied other interesting features of the observed white dwarf luminosity function. In particular, we studied the region around the maximum of the white dwarf luminosity function and we argue that the precise shape of the maximum is best

explained by assuming that the initial-to-final mass relationship is steeper for progenitor masses that are larger than about 4 $M_{\odot}$. We also investigated the presence of a quite apparent bump in the number counts of bright white dwarfs, at $M_{\rm bol} \simeq 10$, which is statistically significant, and which has remained unexplained until now. Our simulations show that this feature of the white dwarf luminosity function is compatible with a recent burst of star formation that occurred about 0.6 ± 0.2 Gyr ago and that is still ongoing. We also found that this burst of star formation was rather intense, about five times stronger than the average star formation rate.

Rowell (2013) find that the shape of the white dwarf luminosity function that was obtained from the SuperCOSMOS Sky Survey (Rowell & Hambly 2011) can be well explained by adopting a star formation rate that presents broad peaks at ~3 Gyr and ~8 Gyr in the past, and marginal evidence for a very recent burst of star formation occurring ~0.5 Gyr ago. However, Rowell (2013) also point out that the details of the star formation history in the solar neighborhood are highly dependent on the adopted cooling sequences and, of course, the adopted observational data set. Since the luminosity function Rowell & Hambly (2011) does not present any prominent feature at bright luminosities, it is natural that they did not found this kind of an episode of star formation. However, Hernandez et al. (2000), using a non-parametric Bayesian analysis to invert the color-magnitude diagram, find that the star formation history presents oscillations with period 0.5 Gyr for lookback times smaller than 1.5 Gyr in good agreement with the results presented here.

In conclusion, the study of volume-limited samples of white dwarfs within the solar neighborhood provides us with a valuable tool to study the history of star formation of the Galactic thin disk. Enhanced and nearly complete samples will surely open the door to more conclusive studies.

Acknowledgements. This work was partially funded by the MINECO grant AYA2014-59084-P and by the AGAUR.

References

Althaus, L. G., García-Berro, E., Isern, J., & Córsico, A. H. 2005, A&A, 441, 689
Althaus, L. G., García-Berro, E., Isern, J., Córsico, A. H., & Rohrmann, R. D. 2007, A&A, 465, 249
Althaus, L. G., Córsico, A. H., Isern, J., & García-Berro, E. 2010, A&ARv, 18, 471
Andrews, J. J., Agüeros, M. A., Gianninas, A., et al. 2015, ApJ, 815, 63
Bedin, L. R., Salaris, M., King, I. R., et al. 2010, ApJ, 708, L32
Bellini, A., Bedin, L. R., Piotto, G., et al. 2010, A&A, 513, A50
Benvenuto, O. G., & Althaus, L. G. 1997, MNRAS, 288, 1004
Bergeron, P., Saffer, R. A., & Liebert, J. 1992, ApJ, 394, 228
Camacho, J., Torres, S., García-Berro, E., et al. 2014, A&A, 566, A86
Catalán, S., Isern, J., García-Berro, E., & Ribas, I. 2008a, MNRAS, 387, 1693
Catalán, S., Isern, J., García-Berro, E., et al. 2008b, A&A, 477, 213
Cojocaru, R., Torres, S., Isern, J., & García-Berro, E. 2014, A&A, 566, A81
Cojocaru, R., Torres, S., Althaus, L. G., Isern, J., & García-Berro, E. 2015, A&A, 581, A108
Dobbie, P. D., Napiwotzki, R., Burleigh, M. R., et al. 2009, MNRAS, 395, 2248
Fontaine, G., Brassard, P., & Bergeron, P. 2001, PASP, 113, 409
García-Berro, E., Ritossa, C., & Iben, Jr., I. 1997, ApJ, 485, 765
García-Berro, E., Torres, S., Isern, J., & Burkert, A. 1999, MNRAS, 302, 173
García-Berro, E., Torres, S., Isern, J., & Burkert, A. 2004, A&A, 418, 53
García-Berro, E., Torres, S., Althaus, L. G., et al. 2010, Nature, 465, 194
García-Berro, E., Torres, S., Althaus, L. G., & Miller Bertolami, M. M. 2014, A&A, 571, A56
Giammichele, N., Bergeron, P., & Dufour, P. 2012, ApJS, 199, 29
Green, R. F., Schmidt, M., & Liebert, J. 1986, ApJS, 61, 305
Hansen, B. M. S., Brewer, J., Fahlman, G. G., et al. 2002, ApJ, 574, L155
Harris, H. C., Munn, J. A., Kilic, M., et al. 2006, AJ, 131, 571
Hernandez, X., Valls-Gabaud, D., & Gilmore, G. 2000, MNRAS, 316, 605
Holberg, J. B., Sion, E. M., Oswalt, T., et al. 2008, AJ, 135, 1225
James, F. 1990, Comput. Phys. Commun., 60, 329
Koester, D., Napiwotzki, R., Christlieb, N., et al. 2001, A&A, 378, 556
Kondo, M., Noguchi, T., & Maehara, H. 1984, Ann. Tokyo Astron. Obs., 20, 130
Kowalski, P. M., & Saumon, D. 2006, ApJ, 651, L137
Kroupa, P. 2001, MNRAS, 322, 231
Lépine, S., & Shara, M. M. 2005, AJ, 129, 1483
Liebert, J., Dahn, C. C., & Monet, D. G. 1988, ApJ, 332, 891
Limoges, M.-M., Lépine, S., & Bergeron, P. 2013, AJ, 145, 136
Limoges, M.-M., Bergeron, P., & Lépine, S. 2015, ApJS, 219, 19
Noh, H.-R., & Scalo, J. 1990, ApJ, 352, 605
Poelarends, A. J. T., Herwig, F., Langer, N., & Heger, A. 2008, ApJ, 675, 614
Press, W. H., Flannery, B. P., & Teukolsky, S. A. 1986, Numerical Recipes. The art of scientific computing (Cambridge: University Press)
Renedo, I., Althaus, L. G., Miller Bertolami, M. M., et al. 2010, ApJ, 717, 183
Rowell, N. 2013, MNRAS, 434, 1549
Rowell, N., & Hambly, N. C. 2011, MNRAS, 417, 93
Salaris, M., Althaus, L. G., & García-Berro, E. 2013, A&A, 555, A96
Salaris, M., Cassisi, S., Pietrinferni, A., Kowalski, P. M., & Isern, J. 2010, ApJ, 716, 1241
Salpeter, E. E. 1955, ApJ, 121, 161
Torres, S., García-Berro, E., Burkert, A., & Isern, J. 2001, MNRAS, 328, 492
Torres, S., García-Berro, E., Burkert, A., & Isern, J. 2002, MNRAS, 336, 971
Torres, S., García-Berro, E., Althaus, L. G., & Camisassa, M. E. 2015, A&A, 581, A90
Tremblay, P.-E., Bergeron, P., & Gianninas, A. 2011, ApJ, 730, 128
Tremblay, P.-E., Ludwig, H.-G., Steffen, M., & Freytag, B. 2013, A&A, 552, A13
York, D. G., Adelman, J., Anderson, Jr., J. E., et al. 2000, AJ, 120, 1579